Available online at www.sciencedirect.com
SCIENCE DIRECT®
ELSEVIER
Ultramicroscopy 95 (2003) 231–238
ultramicroscopy
www.elsevier.com/locate/ultramic

Effects of incidence angles of ions on the mass resolution of an energy compensated 3D atom probe

E. Bémont[a,*], A. Bostel[a], M. Bouet[a], G. Da Costa[a], S. Chambreland[a], B. Deconihout[a], K. Hono[b]

[a] *Groupe de Physique des Matériaux, UMR CNRS 6634, Université et INSA de Rouen 76821 Mont Saint Aignan Cedex, France*
[b] *National Institute for Materials Science, 1-2-1 Sengen, Tsukuba 305-60047, Japan*

Received 1 August 2001; received in revised form 1 February 2002

Abstract

We have used a first-order reflectron lens in an optical tomographic atom probe in order to improve the mass resolution. Calculations have been performed to determine the effect of second-order errors in ion energy and incidence angle on the performance of the lens. By applying a correction procedure based on the results of these calculations, we have been able to improve experimental mass resolution by 30%.

PACS: 29.40.G; 41.85.N; 82.80.R

Keywords: 3D atom probe; Detector; Mass resolution; Reflectron lens; Second-order effects

1. Introduction

The tomographic atom probe (TAP) permits the analysis of conducting materials on a nearly atomic scale [1,2]. Single atoms are field evaporated from a sharp needle specimen. Their chemical nature is identified by time-of-flight mass spectrometry and the position from which they originate at the surface of the specimen is determined using a position-sensitive detector. Thus, a 3D reconstruction of the analysed volume is obtained. Nevertheless, this technique is notably limited by a poor mass resolution. The mass resolution of a conventional 3D atom probe is about 300 at full-width half-maximum (FWHM) and 70 at full-width tenth-maximum (FWTM). This poor mass resolution is due to the energy spread of ions. Indeed, the ions can be field evaporated on the rising edge or the falling edge of the evaporation pulse and thus, not acquire the whole energy provided by the pulse. These energy deficits may be corrected by including an energy compensating system, e.g. a Poschenrieder or a reflectron lens [3–4].

Recently, we have combined an optical tomographic atom probe (oTAP) [5,6,8] with a reflectron lens. For this, we designed a new analysis chamber in collaboration with the National Institute for Materials Science (NIMS) of Tsukuba, Japan. The detector is composed of

*Corresponding author. Tel.: +33-2-35146486; fax: +33-2-35146652.
E-mail address: emilie.bemont@univ-rouen.fr (E. Bémont).

0304-3991/03/$ - see front matter
PII: S0304-3991(02)00321-2

two micro-channel plates (MCP) stack placed in front of a segmented phosphor screen. The anodes of which have their own time-measuring line. The impact position is determined with a fast CCD camera (1 kHz) [6–8].

The spectrometer was designed using first-order approximation (applied for the first time by Cerezo et al. [3]) with respect to energy deficits and the angle of incidence of ions. The first mass spectrum, obtained from the analysis on a Ni-based superalloy, shows a significant improvement in mass resolution. The mass resolution is 580 ± 50 FWHM and 240 ± 15 FWTM. As compared to the conventional 3D atom-probe, the mass resolution is improved by a factor of 4.

In this paper, second-order effects affecting the mass resolution are considered. Theoretical studies are carried out so as to identify all the parameters which may affect the mass resolution. Their influence is quantified, in particular, for the angle of acceptance of the reflectron and for the reflection lens ratio, so as to correct them and significantly improve the mass resolution. Preliminary results, obtained from analyses on a Ni-based superalloy, are presented.

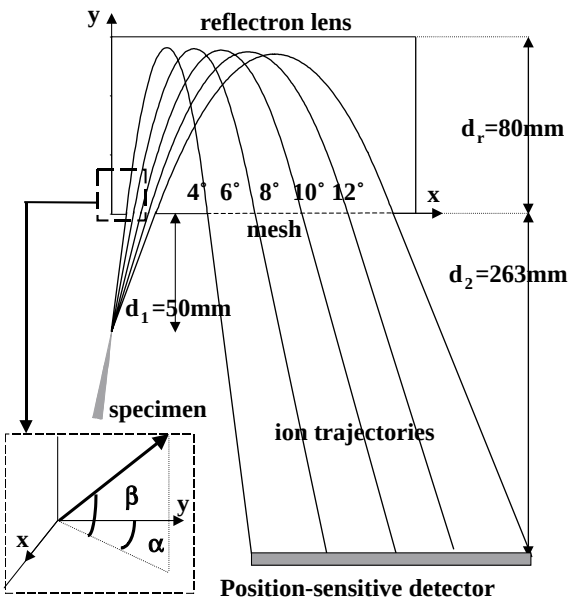

Fig. 1. Principle of the reflectron lens—ion trajectories were calculated with $V_t = 10\,\text{kV}$, $c = 1.02$, $M = m/n = 29\,\text{amu}$, $\delta = 0$.

2. Principle of the reflectron lens

An electric-field-free region and a homogeneous electric-field region, where ions are returned to the detector can model the ions trajectories. The homogeneous electric field in the reflectron is obtained by biasing eight electrodes and a reflector plate. The reflectron can be considered as an electrostatic mirror. Incoming ions with an energy deficit travel with a flight path shorter than that of ions that have the full energy. Time focusing is thus achieved, resulting in an improvement of the mass resolution.

A schematic diagram of the instrument, based on theoretical calculations, is shown in Fig. 1.

2.1. Time-focusing conditions

An ion of a mass m, a charge ne and an energy deficit δ, is evaporated from the specimen at a total voltage V_t and with an angle of emission defined by an azimuthal angle α (ranging from 4° to 12°) and a vertical angle β (ranging from -4° to 4°) . In the field-free region, it travels with a velocity v_0 and its kinetic energy is given by

$$E = \tfrac{1}{2}mv_0^2 = neV_t(1-\delta),$$

so that

$$v_0 = \sqrt{\frac{2neV_t(1-\delta)}{m}}$$

The length of the flight path of the ion being

$$L_{\text{ff}} = \frac{d_1 + d_2}{\cos\alpha\cos\beta} = \frac{d_s}{\cos\alpha\cos\beta},$$

the flight time in this first region is

$$t_{\text{ff}} = \frac{L_{\text{ff}}}{v_0} = \frac{d_s}{\cos\alpha\cos\beta} \times \sqrt{\frac{m}{2neV_t(1-\delta)}}.$$

The ion is accelerated and decelerated through the reflectron lens. Applying the fundamental principle of dynamics and with two successive integrations, we get

$$y(t) = qE\frac{t^2}{2m} + \cos\alpha\cos\beta\sqrt{\frac{2neV_t}{m}} \times t.$$

Then, the flight time through the reflectron lens is

$$t_r = 4d_r \cos\alpha \cos\beta \sqrt{\frac{m}{2neV_t}} \times \frac{V_t}{V_r},$$

with d_r as the physical reflectron depth and $V_r = c \times V_t$ as the voltage applied to the reflector plate of the reflectron.

Finally, the total flight time of the ion is given by Eq. (1)

$$t_t = \sqrt{\frac{m}{2neV_t}} \times \left[\frac{d_s}{\cos\alpha \cos\beta} \times \frac{1}{\sqrt{1-\delta}} + 4d_r \cos\alpha \cos\beta \frac{V_t}{V_r} \sqrt{1-\delta} \right]. \quad (1)$$

In order to achieve the optimum operating condition of the ECoTAP, two ions with the same mass over charge ratio must have the same flight time, whatever their energy deficits are. Then, the first-order condition relative to δ is

$$d_s = 4d_r \cos^2\alpha \cos^2\beta \times \frac{V_t}{V_r}.$$

Time-focusing condition imposes the condition $d_s = 4d_r$, where d_s is the path length in the field-free region and d_r, the depth of the reflectron lens. The physical depth d_r of the reflectron ($d_r = 80$ mm) is larger than the d_r value imposed by the focusing condition. d_r is set to the theoretical value by applying a voltage V_r on the reflector plate slightly larger than V_t. The lens ratio is defined by $c = V_r/V_t$. Given the actual values of d_r and d_s, c has to be settled to 1.02 to achieve the focusing condition. The value of c can be adjusted around this theoretical value in order to correct for possible derivation of d_r and d_s values.

The geometric features of the reflectron lens were determined by considering the first-order condition relative to δ and an angle of acceptance null, leading to $d_s = 4d_r$. However, the effect of incidence angles of ions modifies the time-focusing condition. There is not only one optimum condition but one by couple $(\alpha;\beta)$.

3. Study of second-order effects on the mass resolution

3.1. Effects of the energy deficit δ

We must ensure that the first-order approximation on δ is sufficient to determine good geometric features of the reflectron lens. In this aim, we can compare the influence on the mass resolution of first- and second-order approximations on δ. Consider Eq. (1). The time difference between first- and second-order is given by

$$\Delta t_t = \sqrt{\frac{m}{2neV_t}} \times \frac{\delta^2 d_r}{8\cos\alpha\cos\beta} \times \left(12 - \frac{\cos^2\alpha\cos^2\beta}{c}\right).$$

The contribution of energy deficits to the mass resolution can be derived from the width of mass peaks in a straight atom probe [7]. If the mass resolution is measured at FWTM, $\delta = 1.3\%$. This energy deficit leads to a time difference Δt_t less than 200 ps. Using the second-order condition, the mass resolution would be increased by less than 5%. As it will be shown, this can be neglected as compared to the contribution of the ion emission angles. The first-order approximation on δ is sufficient to derive good geometric features for the reflectron lens and achieve a significant improvement of the mass resolution.

3.2. Influence of the angles of emission α and β

In order to study the flight time dependence on the emission angles of the ions, we can calculate the flight times as a function of α and β. Errors on time and voltage measurements are supposed to be null and ions have the full energy ($\delta = 0$). It is then possible to build a mass spectrum showing the contribution of α and β alone.

By using Eq. (1) where the condition $ds = 4\,dr$ is realised, we consider ions with a mass-over-charge ratio of 29 amu ($^{58}Ni^{2+}$ ions). The total voltage applied to the specimen V_t and the reflection lens ratio c are constant, respectively, fixed to 10 kV and 1.02. All these parameters will be kept for further calculations. Each ion is associated with a

particular couple $(\alpha;\beta)$. Then, the flight time of each ion is calculated. This one depends on the impact position on the detector and consequently, on the emission angles of the ion.

As expected, α has a stronger influence on the flight time than β. Hence, angle effects are essentially due to the horizontal angle α.

The maximum time difference on the detector is of 0.6 ns. Mass resolution is thus limited around 2200 at the base of the peak. This time spread is comparable to the 0.5 ns precision of the timers. From the measured impact position on the detector, α and β can be deduced so that this time spread can easily be corrected.

The same study was conducted using PC Simion3D 6.0 Software. These simulations are more realistic than our theoretical result and they give a maximum time difference larger than 5 ns. In fact, the influence of the angle of emission is probably larger than that given by our calculations, indicating that angles effects must not be neglected.

To observe the influence of α and β on the mass resolution, theoretical mass spectra were plotted for various angles α (Fig. 2). We notice a shift of the $^{58}Ni^{2+}$ mass peak as α increases. For an angle α ranging from 4° to 12°, the peak maximum, in this case, is shifted by 0.01 amu. This explains why mass resolution is limited by the angle of incidence of the ions. If this mass shift was properly corrected, the FWHM and FWTM mass resolutions could be improved. When mass spectra are plotted for different β values, no peak shift

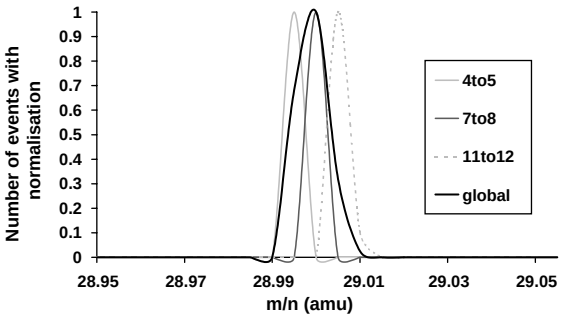

Fig. 2. Theoretical mass spectra for different values of α—calculation parameters: $V_t = 10$ kV, $c = 1.02$, $M = 29$ amu, $\delta = 0$—errors in V_t and t_t measurement are neglected.

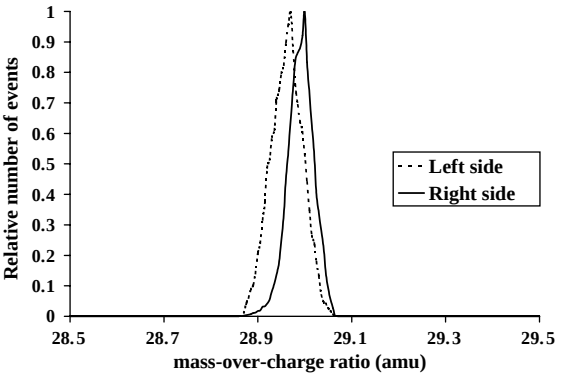

Fig. 3. Experimental mass spectra plotted for ions collected on the right and the left side of the detector.

appears. Again, this shows that β has a minor influence.

Fig. 3 shows the shift of the $^{58}Ni^{2+}$ mass peak as the angle α increases for the experimental mass spectrum measured from the analysis of a Ni-based superalloy. To underline this effect, two mass spectra were plotted, the first for ions striking the left side of the detector (α from 4° to 8°) and the second, for ions striking the other side (α from 8° to 12°). This experimental result tends to show that our theoretical calculation is realistic but underestimates the angle effects (the experimental mass spectrum exhibits a shift of the $^{58}Ni^{2+}$ mass peak 4 times larger than that given by our calculations).

3.3. Combination of influences of the energy deficit and of the emission angles

Here, the influence of the energy deficit δ is combined with the effects of the emission angles α and β. This study was conducted with two different couples $(\alpha;\beta)$, the worse case (12°;4°) and the best case (4°;0°). The flight time, in both cases, shows variations which prove the importance of the angle of emission (Fig. 4). Indeed, for $\delta = 1.3\%$ corresponding to FWTM, the whole variation is about 1 ns. So, by taking into account the energy deficits, there is a additional loss in mass resolution.

In conclusion, the angle of emission leads to a widening of the $^{58}Ni^{2+}$ mass peak because of the

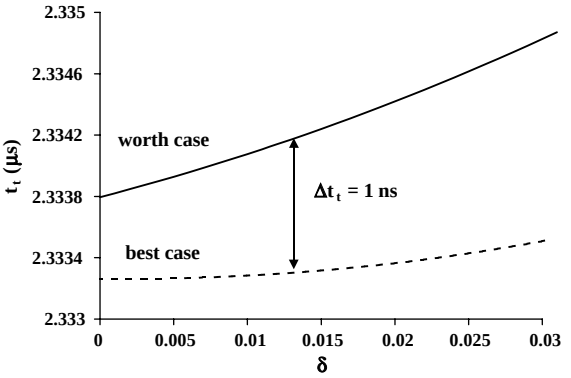

Fig. 4. Flight time variations with the energy deficit δ in the worse case ($\alpha = 12^\circ; \beta = 4^\circ$) and the best case ($\alpha = 4^\circ; \beta = 0^\circ$).

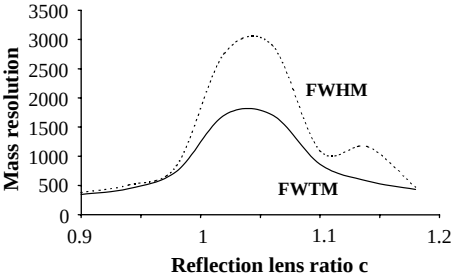

Fig. 5. Theoretical variations of FWTM and FWHM mass resolutions with the reflection lens ratio—calculation parameters: $V_t = 10\,\text{kV}$, $M = 29\,\text{amu}$, $\delta = 0$.

shift due to the angle of emission. This effect is all the more pronounced as the energy deficit is large.

3.4. Influence of the reflection lens ratio c

If the lens ratio c is different from the theoretical value given by the equation $\mathrm{d}s = 4\mathrm{d}r$, the optimum time-focusing condition is not achieved. Indeed, the ratio c fixes the real depth of the reflectron lens, i.e. the position of the equipotential where ions are reflected. Its theoretical value c_{th} is given by the geometric features of the device. In our case, c_{th} is of 1.02 since $d_s = 313\,\text{mm}$ and the physical value of d_r is 80 mm.

The influence of the reflection lens ratio on the mass resolution is studied by plotting a theoretical mass spectrum, as in the previous section, for different values of the lens ratio c, α ranging from 4° to 12° and β, from -4° to 4°. FWHM and FWTM mass resolutions were calculated for each $^{58}Ni^{2+}$ mass peak (Fig. 5).

We observe that the mass resolution is very dependent on the value of c. Note a maximum for $c = 1.04$. If the effects of the emission angles are not corrected, the optimum focusing condition is achieved for a value of c different from c_{th}.

This approach does not quantify the effect of a small variation of the reflection lens ratio on the flight time. By plotting the flight time of a $^{58}Ni^{2+}$ ion versus the reflection lens ratio c, we notice that a variation of 0.01 of c induces an averaged time variation of 10 ns. The angle of emission was chosen so as to maximise the effect ($\alpha = 12^\circ$; $\beta = 4^\circ$). However, it shows that because two power supplies are used to bias the specimen and the lens, these power supplies have to be as stable as possible. As a result, a hardware control of V_r and V_t will lead to a better mass resolution than a software control of those voltages.

3.5. Detection effects

The detector used in our case is composed of 16 independent anodes. So, 16 independent time-measuring lines are required [8]. However, from one line to another, a systematic delay can exists due to the variation of the length of cables, to the transit times in the discriminators, etc. It means that a calibration between channels is necessary to be able to correct the transit time spread in the time-of-flight measurement. In order to measure this spread, two flight times were measured for each event: on the MCP and on the strip that is triggered on the segmented phosphor screen. A constant number of virtual $^{58}Ni^{2+}$ ions (generated by a pulse generator) were sent on the measuring line. The time difference $\Delta t = t_{MCP} - t_{strip}$ has been measured. The experiment was conducted for each strip. The result obtained for 3 strips is shown in Fig. 6.

The time difference distribution for each strip follows a Gaussian distribution as expected (this shape is representative of the uncertainty of the timers which is of 0.5 ns). Nevertheless, we notice a shift of the curves from one strip to another. This phenomenon is explained by the fact that each

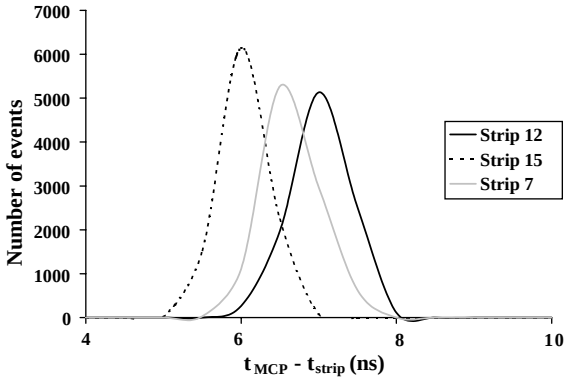

Fig. 6. Distributions of the difference between flight time measurement on the MCP and on the strips.

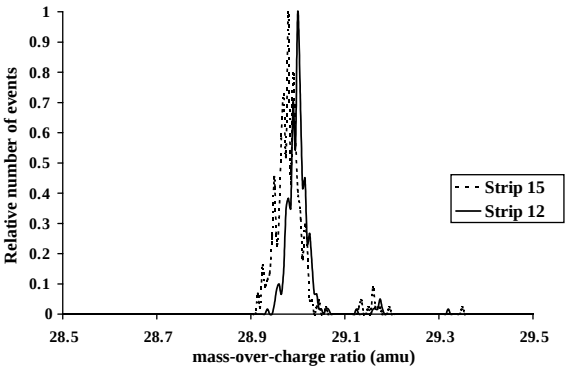

Fig. 7. Experimental mass spectra from the analysis on a Ni-based superalloy plotted for ions collected on strip #12 and strip #15.

time-measuring line has its own propagation time, depending on the features of the components. Each line has a fixed shift, which is at worse of 1 ns. Consequently, the inaccuracy on the flight time is not only due to the timers but also due to the measuring lines. This result was experimentally observed and Fig. 7 shows the shift of the $^{58}Ni^{2+}$ mass peak from one strip to another for the experimental mass spectrum.

Once the delay induced by each line is quantified, the correction can easily be done, since this error is systematic. This calibration procedure appears necessary in order to still improve the mass resolution.

Another detection effect has to be taken into account. Each strip consists of a thin layer of a

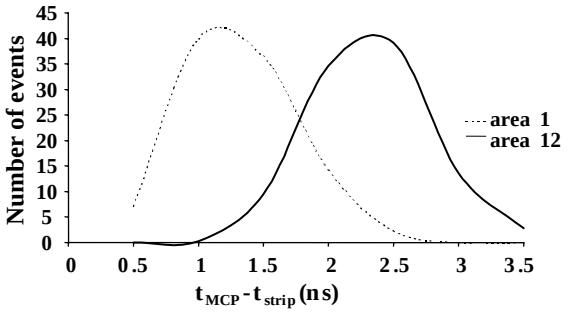

Fig. 8. Distribution of the flight time difference in the nearest and the farthest area from the connection.

semi-conduct material (ITO) [8]. Because of the resistivity (20 Ω square) of ITO, strip resistance can reach 500 Ω. In addition, surfaces facing are large so that stray capacitance exist (for example, MCP/strip). This leads to a widening of the electric signals. So, the resistance of the strips and the existence of capacitance have an influence on the flight time measurement according to the distance between the impact position on the strip and the measuring connections. To check this aspect, a strip was divided into 12 areas. From experimental data, the time difference between signals measured on the MCP and those measured on the strip was evaluated as a function of the impact position along the strip. The area in which the impact occurred was determined. Fig. 8 shows the distribution of the time difference measured into two areas.

Area 1 is the closest to the connection and area 12, the farthest. For each area, the flight time has an uncertainty of about ± 0.5 ns, which conforms to the errors of the timers. Between the two extremities, we find a time difference of 1.5 ns. This value corresponds to the propagation time through the strip.

So, there is a systematic error on the flight time measured on strips, depending on the distance impact position/measuring connections.

In this section, we have demonstrated that the error on flight time measurement is about 2 ns. By the quantification of the effects leading to this error, we are now able to correct them and to reduce it to 0.5 ns. The corresponding gain in mass resolution is significant.

4. Summary

In this study, we have examined some of the parameters that affect the mass resolution in an optical 3D atom-probe including a reflectron lens. We have identified them and quantified their influence on the mass resolution. The emission angles of the ions and the reflection lens ratio are important parameters contributing to the mass resolution degradation. Indeed, we have shown that the angles $(\alpha;\beta)$, intrinsic to the configuration of the instrument, induce a shift of the mass peak which participate to the degradation of the mass resolution. The reflection lens ratio is of course a fundamental parameter since it fixes the time-focusing condition. It determines the ions trajectories through the reflectron lens. The mass resolution is consequently very dependent on this parameter. Great care must be taken to fix the value of c. Then, we have quantified some errors inherent to the detection itself. We are now able to reach a significant improvement in mass resolution.

Very preliminary results from analyses on a Ni-based superalloy are in good agreement with our theoretical calculations. Currently, we are able to correct angle effects by software, as shown in Fig. 9b. We are able to achieve a mass resolution around 700 FWHM and 350 FWTM. The corresponding gains in mass resolutions are of

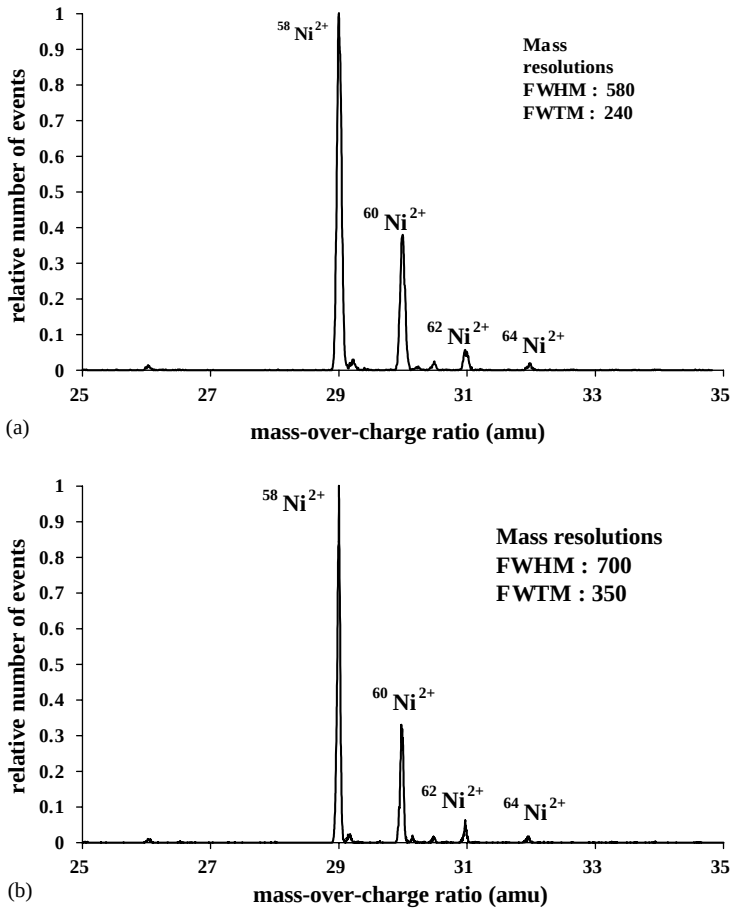

Fig. 9. Experimental mass spectrum from the analysis on a Ni-based superalloy before (a) and after (b) correction of angle effects—experimental conditions: $V_r \approx 10\,\text{kV}$, $c = 1.06$, coupling factor 75%, pulse fraction 25%.

20% FWHM and 45% FWTM as compared to the raw mass spectrum (Fig. 9a). The improvement of the mass resolution is already significant. This corrected mass spectrum (shown in Fig. 9b) was plotted for one strip. We may improve the mass resolutions to 1100 FWHM and 400 FWTM. But the number of collected ions is not large enough to obtain a significant result.

Further studies will consist in taking into account the grid placed 12 mm in front of the detector. Since the grid induces a post-acceleration of ions, the region between the grid and the detector cannot be considered in calculations as a free electric-field region.

References

[1] D. Blavette, B. Deconihout, A. Bostel, J.M. Sarrau, M. Bouet, A. Menand, Rev. Sci Instrum. 64 (1993) 2911.
[2] D. Blavette, B. Deconihout, A. Bostel, J.M. Sarrau, A. Menand, C. R. Acad. Sci. Paris, 317(II) (1993) 1279–1280.
[3] A. Cerezo, T.J. Godfrey, S.J. Sijbrandij, G.D.W. Smith, P.J. Warren, Rev. Sci. Instrum. 69 (1998) 49.
[4] W. Drachsel, L.V. Alvensleben, A.J. Melmed, J. Phys. (Paris) 50 (1989) C8–541.
[5] M.K. Miller, Surf. Sci. 266 (1992) 494.
[6] B. Deconihout, L. Renaud, G. Da Costa, M. Bouet, A. Bostel, D. Blavette, Ultramicroscopy 73 (1998) 253–260.
[7] B. Deconihout, A. Menand, M. Bouet, J.M. Sarrau, Surf. Sci. 266 (1991) 523–528.
[8] L. Renaud, Ph.D. Thesis, University of Rouen, 2001 (Chapter II).